1-1-2003

Narrowband interference excision in hybrid frequency-hopping/ direct-sequence spread-spectrum systems

Carlos Jaime Chávez
Iowa State University

Narrowband interference excision in hybrid frequency-hopping/direct-sequence spread-spectrum systems

by

Carlos Jaime Chávez

A thesis submitted to the graduate faculty

in partial fulfillment of the requirements for the degree of

MASTER OF SCIENCE

Major: Electrical Engineering

Program of Study Committee:
Aleksandar Dogandzic, Major Professor
Steve F. Russell
Peter J. Sherman

Iowa State University

Ames, Iowa

2003

Graduate College
Iowa State University

This is to certify that the master's thesis of

Carlos Jaime Chávez

has met the thesis requirements of Iowa State University

Signatures have been redacted for privacy

TABLE OF CONTENTS

INTRODUCTION

Direct-sequence spread-spectrum (DSSS) systems are used in a wide range of applications. Such systems were originally developed for military communications, but DSSS systems are now prolific in civilian communications as well. These systems are generally used in four types of applications. These include low probability of intercept (LPI) signaling, anti-jam (AJ) signaling, code division multiple access (CDMA), and communication over multipath channels.

Regardless of the application, a DSSS signal uses a physical bandwidth much greater than the information bandwidth. As a result, a DSSS receiver must be capable of receiving a wideband signal. Unfortunately, this makes a DSSS receiver vulnerable to being desensitized by high-power narrowband signals within its wide received bandwidth. A solution to this problem is to detect the interfering signals and remove them from the received bandwidth in a process called narrowband interference excision. A number of techniques exist to accomplish this. Once narrowband interference excision has been performed, conventional DSSS methods can be used to demodulate the desired signal.

However, some systems combine DSSS with frequency-hopping spread-spectrum (FHSS) techniques. This may be done to enhance the LPI, AJ, or multipath performance of the communication system. Such a hybrid frequency-hopping/direct-sequence spread-spectrum (FH/DSSS) system complicates any narrowband interference excision solution. This is because the FH/DSSS receiver is continually

presented with a new interference environment every time it hops to a new carrier frequency.

This thesis investigates one technique for narrowband interference excision for application in a hybrid FH/DSSS system. This technique is based on the discrete Fourier transform (DFT). An overview of DFT-based narrowband interference excision is given. This includes a brief discussion of excision algorithms and the overlap-and-add architecture used to mitigate the effects of windowing on the time-domain waveform.

Next is a discussion of the properties of window functions that determine the performance of the DFT-based excision technique. These critical properties are windowing loss, excision loss, and interference rejection. Windowing loss is the loss in signal-to-noise ratio (SNR) resulting from the time-domain shape of the window function. Excision loss is the loss due to excising part of the desired signal in the process of excising the interference. Interference rejection is the reduction in interference power as a result of excision. A method to determine excision loss and interference rejection has been developed for the special case of a four-term cosine series window function (Young and Lehnert, March 1999). This thesis presents a general method for computing excision loss and interference rejection for any window function.

Finally, the application of DFT-based excision in a hybrid FH/DSSS system is explored. The critical element is the transient nature of the interference as seen by the excision processing. This determines the maximum length of the window function.

Once this is known, a performance trade-off can be made between loss and interference rejection.

At the end of this thesis is an appendix containing the Matlab® code used to produce the results presented here. Also, a list of references is given.

OVERVIEW OF DFT-BASED EXCISION

Figure 1 depicts a DFT-based narrowband interference excision technique. This method uses a windowed real-time DFT to obtain a frequency-domain representation of the received signal. The DFT bins containing interference are identified and excised by means of an appropriate excision algorithm. A real-time IDFT is used to reconstruct the received signal with the interfering signals removed. Two signal paths are used in a 50% overlap-and-add architecture to mitigate the effects of windowing on the time-domain waveform (Young and Lehnert, 1999). With the narrowband interference removed, the excised signal can be processed using conventional direct-sequence spread spectrum demodulation techniques.

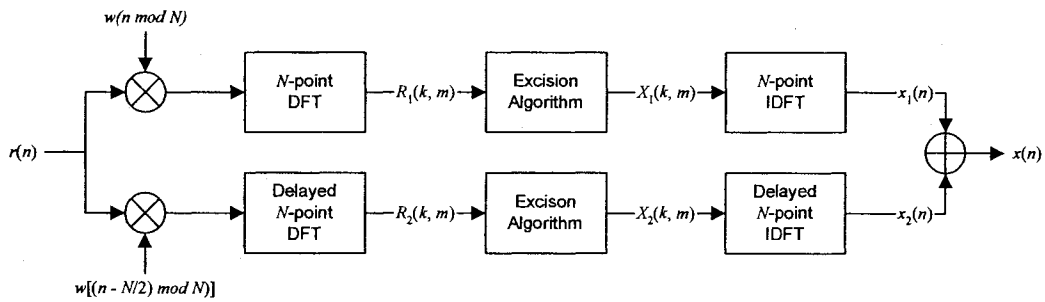

Figure 1. 50% Overlap-and-Add DFT-Based Excision

In the upper path in Figure 1, the received discrete-time signal $r(n)$ is periodically multiplied by the window function $w(n)$ of length N. In general, $r(n)$ is a complex signal, with an in-phase and a quadrature part. The window function can be selected from a wide range of well known window functions used in spectral analysis.

A real-time N-point DFT operation is performed on the windowed version of the received signal. The DFT is defined as follows:

$$DFT[x(n)] = X(k) = \sum_{n=0}^{N-1} x(n)e^{-j2\pi kn/N}$$

where $k = 0, 1, 2, \ldots, N - 1$ (Proakis and Manolakis, 1996).

The windowed DFT operation results in the periodogram $R_1(k, m)$ as shown below:

$$R_1(k, m) = DFT[w(n)r(n + Nm)]$$

Note that $R_1(k, m)$ represents the kth frequency bin of the DFT at time m where $k = 0, 1, 2, \ldots, N - 1$. Time m refers to the DFT of $r(n)$ over the time interval $n = Nm, Nm + 1, Nm + 2, \ldots, Nm + N - 1$, where $m = 0, 1, 2, \ldots$ The periodogram $R_1(k, m)$ can also be viewed as a collection of N discrete-time signals that are the outputs of N bandpass filters that have been decimated by N.

With the spectral estimate $R_1(k, m)$ as its input, the excision algorithm shown in Figure 1 identifies the frequency bins that contain energy from high-power narrowband interference and excises those corrupted bins. This produces the excised periodogram $X_1(k, m)$. Many excision algorithms have been suggested for use in DFT-based excision methods. These include fraction zeroize, threshold zeroize, fraction clip, noise clip, fraction clip to threshold, and optimum clip (Young and Lehnert, 1998).

This thesis assumes some variation of the threshold zeroize excision algorithm. For this method, a power estimate is computed for each frequency bin k of

$R_1(k, m)$ at time m. The threshold zeroize algorithm sets the value of any frequency bin to zero when that bin's power exceeds some threshold (Young and Lehnert, 1998). Thus, $X_1(k, m) = R_1(k, m)$, except for any excised bins, whose values are zero. Any number of methods can be employed to arrive at the threshold used in this algorithm. However, it is sufficient for the purposes of this thesis simply to assume some known threshold.

Once the excised spectral estimate $X_1(k, m)$ is computed, the real-time N-point IDFT operation shown in Figure 1 reconstructs an excised version of the windowed input signal. The IDFT is defined as follows:

$$IDFT[X(k)] = x(n) = \frac{1}{N}\sum_{k=0}^{N-1} X(k)e^{j2\pi kn/N}$$

where $n = 0, 1, 2, \ldots, N - 1$ (Proakis and Manolakis, 1996).

The IDFT operation results in the reconstructed signal $x_1(n)$ as shown below:

$$x_1(n + Nm) = IDFT[X_1(k, m)]$$

Note that $x_1(n)$ is an excised version of the received signal $r(n)$ with high-power narrowband interference removed. However, unlike $r(n)$, $x_1(n)$ is modulated by the window function $w(n)$. If no interference were present in $r(n)$, and no DFT bins were excised, $x_1(n)$ could be expressed as follows:

$$x_1(n) = w(n \bmod N)r(n)$$

The upper graph in Figure 2 shows $x_1(n)$ for a constant valued $r(n)$ and a triangular window function $w(n)$ when no DFT bins are excised. Clearly, the window function results in significant distortion, even when no excision is performed. To

mitigate this effect of windowing on the time-domain waveform, the received signal $r(n)$ is processed through a second signal path, as depicted in Figure 1.

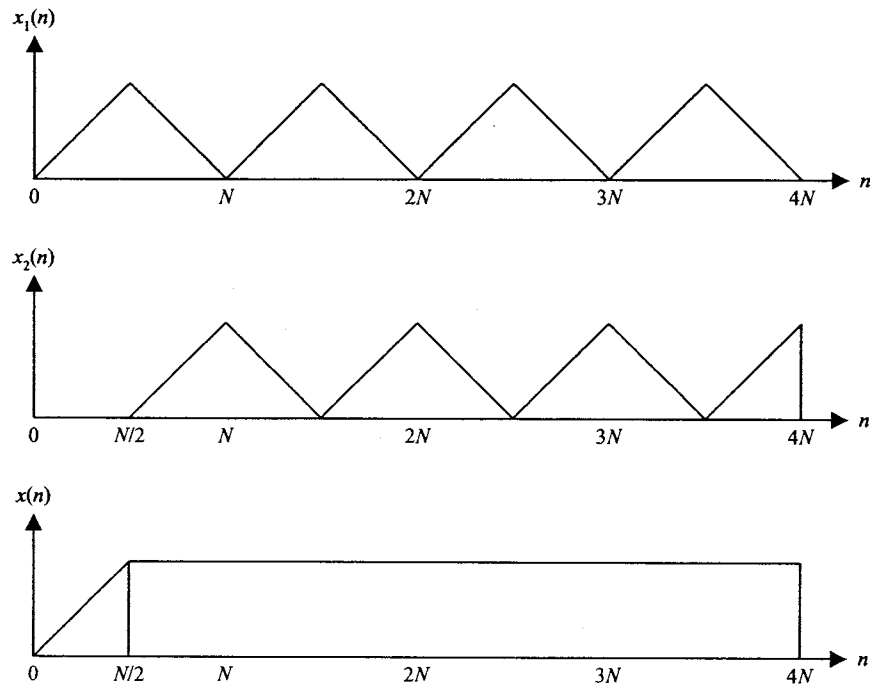

Figure 2. Time Domain Waveforms for 50% Overlap-and-Add

The signal processing in the lower path shown in Figure 1 is identical to that of the upper path, except that the window function, DFT operation, and IDFT operation are delayed by half the window length, or $N/2$ samples. Note that the signal $r(n)$ is not delayed. The windowed N-point DFT operation results in the periodogram $R_2(k, m)$ as follows:

$$R_2(k, m) = DFT[w(n)r(n + Nm + N/2)]$$

The excision algorithm produces the periodogram $X_2(k, m)$ from the spectral estimate $R_2(k, m)$ as described previously. The N-point IDFT operation results in the reconstructed signal $x_2(n)$ as shown below:

$$x_2(n + Nm + N/2) = IDFT[X_2(k, m)]$$

Once $x_1(n)$ and $x_2(n)$ have been computed, they are summed together to produce the final excised signal $x(n)$, as shown in Figure 1. If no interference were present in $r(n)$, and no DFT bins were excised, $x_2(n)$ could be expressed as follows:

$$x_2(n) = w[(n - N/2) \bmod N]r(n)$$

The signal $x(n)$ is simply the sum of the two signals $x_1(n)$ and $x_2(n)$. Once again, if no interference were present in $r(n)$, and no DFT bins were excised, $x(n)$ could be expressed as follows:

$$x(n) = x_1(n) + x_2(n) = \{w(n \bmod N) + w[(n - N/2) \bmod N]\}r(n)$$

The middle graph in Figure 2 shows $x_2(n)$ for a constant valued $r(n)$ and a triangular window function $w(n)$ when no DFT bins are excised. The lower graph in Figure 2 shows $x(n) = x_1(n) + x_2(n)$. While both $x_1(n)$ and $x_2(n)$ are significantly distorted versions of the received signal $r(n)$, this effect has been eliminated in the signal $x(n)$. This shows how a 50% overlap-and-add architecture mitigates the effects of windowing on the time domain waveform. The extent to which this distortion is reduced depends upon the window function used.

PROPERTIES OF WINDOW FUNCTIONS

The particular window function $w(n)$ employed is of critical importance in the DFT-based narrowband interference excision technique described previously. The window function can be selected from a wide range of well know window functions used in spectral analysis. One broad class of window functions is the four-term cosine series window. This class includes the rectangular, Hamming, Hanning, and Blackman-Harris windows, among others. These windows can be described by the following expression:

$$w(n) = \sum_{i=0}^{3} a_i (-1)^i \cos\left(\frac{2\pi i n}{N}\right)$$

given appropriate coefficients a_i and the window length N (Harris, 1978). The four-term cosine series class of windows has been examined in some depth in the context of narrowband interference excision (Young and Lehnert, 1999).

Another popular window function used in both spectral analysis and digital filter design is the Kaiser window. This window function is defined as follows:

$$w(n) = \frac{I_0\left(\alpha\sqrt{1-\frac{\left(n+\frac{1}{2}-\frac{N}{2}\right)^2}{\left(\frac{N}{2}\right)^2}}\right)}{I_0(\alpha)}$$

assuming even length N and where $I_0(\cdot)$ is the modified Bessel function of the first kind and 0^{th} order (Orfanidis, 1996).

The Kaiser window has the advantage of being continuously adjustable using the shape parameter α. This makes the Kaiser window a flexible choice for use with a DFT-based excision technique.

Whatever the choice of window function, three properties describe how a given window function affects the performance of a DFT-based excision system. These properties are windowing loss, excision loss, and interference rejection. Windowing loss describes the loss in performance due to the time-domain shape of the window function. Excision loss is the loss due to excising part of the desired signal in the process of excising the interference. Interference rejection quantifies the reduction in interference power as a result of excision.

Windowing Loss

Windowing loss is the loss in signal-to-noise ratio (SNR) resulting from the time-domain shape of the window function. This corresponds to the loss incurred when no interference is present in the received signal $r(n)$ and no DFT bins are excised. Windowing loss is computed as follows. The noise power gain G_{NP} and the peak power gain G_{PP} of a window function $w(n)$ of length N are defined as shown below (Harris, 1978):

$$G_{NP} = \frac{1}{N}\sum_{n=0}^{N-1} w^2(n)$$

$$G_{PP} = \left[\frac{1}{N}\sum_{n=0}^{N-1} w(n)\right]^2$$

The effective noise bandwidth (ENBW) of a window function is the ratio of the noise power gain to the gain experienced by the desired signal (Harris, 1978):

$$\text{ENBW} = G_{NP}/G_{PP}$$

Assuming additive white Gaussian noise (AWGN), the ENBW (in DFT bins) of a window function represents the loss in SNR due to the window shape, and is thus equal to the windowing loss L_w (Young and Lehnert, 1999):

$$L_w = G_{NP}/G_{PP}$$

This expression for windowing loss quantifies the effects of the time-domain shape of the window function. As discussed previously, an overlap-and-add excision architecture can reduce this loss. To compute the windowing loss for a 50% overlap-and-add architecture, an effective window function $w_e(n)$ must be computed as follows:

$$w_e(n) = w(n) + w[(n - N/2) \bmod N]$$

This effective window function accounts for both signal paths depicted in Figure 1 and is simply the sum of the window function $w(n)$ and a circularly delayed version of the window function. The effective window function $w_e(n)$ can be substituted for the window function $w(n)$ in the previously described computations to arrive at the windowing loss L_w when using a 50% overlap-and-add architecture.

Windowing loss L_w was computed for several four-term cosine series window functions of length $N = 256$ using the method described. Table 1 summarizes these results, including the windowing loss (in dB) with and without 50% overlap-and-add. Note that the windowing loss can be significantly reduced, if not eliminated, using a

50% overlap-and-add architecture. These results agree with previous analysis of these window functions (Young and Lehnert, 1999).

Table 1. Windowing loss for four-term cosine series window functions ($N = 256$)

Window Function	L_w (dB)	L_w (dB) with 50% overlap-and-add
$\cos^4$	2.89	0.23
Blackman-Harris, -74 dB side lobes	2.53	0.12
Hanning	1.76	0
Hamming	1.34	0
Rectangular	0	0

Windowing loss was also calculated for several Kaiser window functions of length $N = 256$ for various values of the shape parameter α. Table 2 summarizes these results, including the windowing loss (in dB) with and without 50% overlap-and-add. Once again, the windowing loss can be significantly reduced by employing a 50% overlap-and-add architecture.

Table 2. Windowing loss for Kaiser window functions ($N = 256$)

Window Function	L_w (dB)	L_w (dB) with 50% overlap-and-add
Kaiser ($\alpha = 9.5$)	2.56	0.13
Kaiser ($\alpha = 8.5$)	2.34	0.07
Kaiser ($\alpha = 7.5$)	2.09	0.03
Kaiser ($\alpha = 6.5$)	1.81	0.01
Kaiser ($\alpha = 5.5$)	1.50	0.00

In summary, windowing loss is the reduction in SNR resulting from the time-domain shape of a given window function. This loss is always incurred in a DFT-based excision system, whether interference is excised or not. However, as illustrated by the results in Table 1 and Table 2, windowing loss can be dramatically reduced using a 50% overlap-and-add excision architecture.

Excision Loss

Excision loss is the loss due to excising part of the desired signal in the process of excising the interference. Assuming the threshold zeroize excision algorithm referred to previously, any DFT bin is set to zero if it contains interference power exceeding some threshold. While these excised bins contain significant interference power, they contain some of the desired signal power as well. This removal of desired signal power will result in some loss in performance. Because this loss depends on the particular characteristics of the desired signal, it is useful to consider excision loss simply in terms of the number of DFT bins excised given an interfering signal.

A method to determine the number of DFT bins excised has been developed for the special case of a four-term cosine series window function (Young and Lehnert, 1999). This method derives an expression for the number of DFT bins whose powers exceed a given threshold for a single interfering tone and a given window function. The main lobe of the DFT consists of those bins which exceed the threshold. The mean main lobe width vs. threshold is computed for a given window function,

assuming a uniformly distributed interference frequency. The mean main lobe width, in DFT bins, is the mean number of bins that are excised for the given threshold. Thus, mean main lobe width can be used as a measure of excision loss.

A general method for computing mean main lobe width for a particular window function, a given threshold, and a single-tone interferer is presented here. The spectrum $W(\omega)$ of the window function $w(n)$ can be computed using the Fourier transform as follows (Proakis and Manolakis, 1996):

$$W(\omega) = \sum_{n=0}^{N-1} w(n) e^{-j\omega n}$$

An indicator function $I_w(\omega, T)$ is defined for the window function $w(n)$ as shown here:

$$I_w(\omega, T) = \begin{cases} 1, & |W(\omega)|^2 > T \\ 0, & |W(\omega)|^2 \leq T \end{cases}$$

This function indicates whether or not the power spectrum $|W(\omega)|^2$ of the window function $w(n)$ exceeds the excision threshold T at a given frequency ω.

The main lobe width $M_w(T)$ for the window function $w(n)$, as a function of the threshold T, is computed by integrating the indicator function $I_w(\omega, T)$ over the frequency ω:

$$M_w(T) = \frac{N}{2\pi} \int_{-\pi}^{\pi} I_w(\omega, T) d\omega$$

The integral is scaled by $N/2\pi$ to obtain the main lobe width in DFT bins for a window function of length N.

The main lobe width $M_w(T)$ calculated here is the main lobe width of the power spectrum of the window function $w(n)$, given the threshold T. A single-tone interferer modulated by the window function $w(n)$ has a power spectrum identical to that of the window function shifted to the frequency of the interferer. As a result, $M_w(T)$ is also the main lobe width of the power spectrum of a single-tone interferer windowed by $w(n)$. Thus, $M_w(T)$ is the mean main lobe width, in DFT bins, of the DFT of a single-tone interferer windowed by the function $w(n)$ of length N, given the excision threshold T. As such, the mean main lobe width $M_w(T)$ is as a measure of excision loss in terms of the number of DFT bins excised.

The main lobe width $M_w(T)$ can be easily evaluated numerically. The Matlab® computing environment produced by MathWorks, Inc. was used to achieve this. The code used to produce the results given here can be found in the appendix.

Figure 3 shows the mean main lobe width vs. excision threshold for several four-term cosine series window functions. The threshold is normalized to the power present in a single tone interferer with no window applied. Window functions of length $N = 256$ were used in these computations, and 2048 equally spaced frequencies per DFT bin were used to approximate the power spectrum of the window function. It is worth noting that the window length N has no significant effect on these calculations if N is much greater than the main lobe widths of interest. The results in Figure 3 were produced using the method described here and agree with the results given by the special-case method referred to previously (Young and Lehnert, 1999).

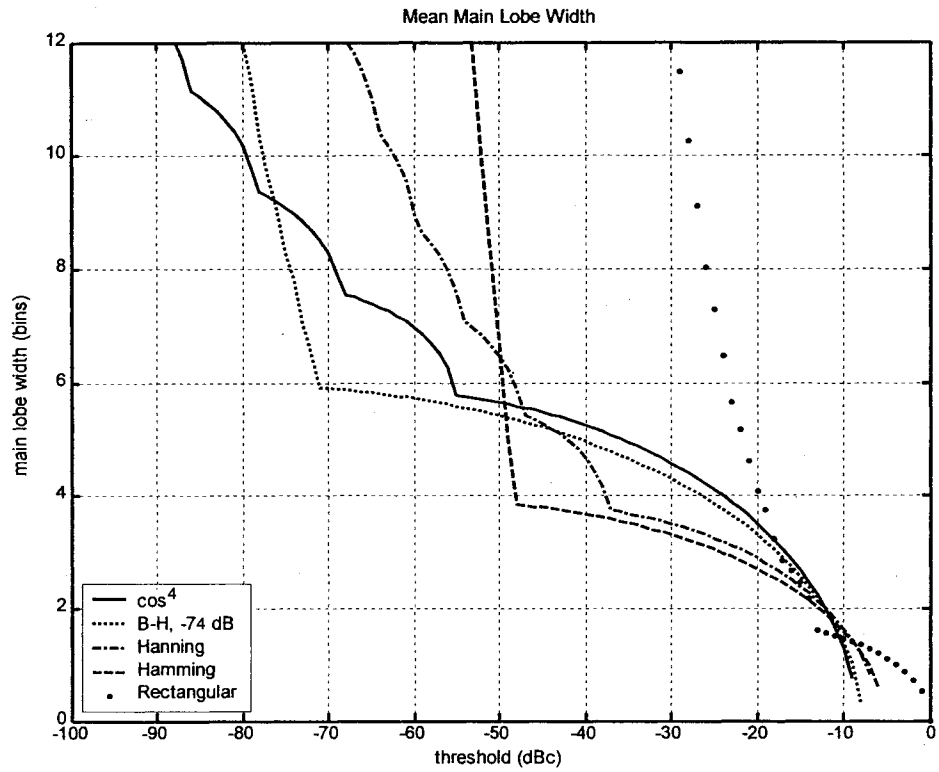

Figure 3. Mean main lobe width vs. threshold for 4-term cosine series windows ($N = 256$)

Some comparisons can be made in examining Figure 3. First, note that the rectangular window is almost completely unsuitable for use in a DFT-based excision technique. For thresholds lower than -13 dBc, the main lobe width of the rectangular window increases rapidly. By comparison, the Hamming window performs much better in terms of main lobe width. The mean number of DFT bins excised using a Hamming window is less than 4 for thresholds down to -48 dBc. However, for thresholds below -48 dBc, the main lobe width of the Hamming window dramatically

increases. The Blackman-Harris (B-H) window shown Figure 3 has a wider main lobe than the Hamming window, but its main lobe width remains under 6 bins for thresholds all the way down to -71 dBc. Summarizing, each window exhibits a breakpoint in excision threshold above which the main lobe width is well behaved, and below which the main lobe rapidly expands. This breakpoint is essentially the lowest threshold for which a given window function is useful in a DFT-based excision scheme. In general, windows with narrower main lobes exhibit higher threshold breakpoints.

Figure 4 shows the mean main lobe width vs. excision threshold for several Kaiser window functions for various values of the shape parameter α. Once again, the threshold is normalized to the power present in a single tone interferer with no window applied. Window functions of length $N = 256$ were used in these computations, and 2048 equally spaced frequencies per DFT bin were used in the approximation of the power spectrum of the window function.

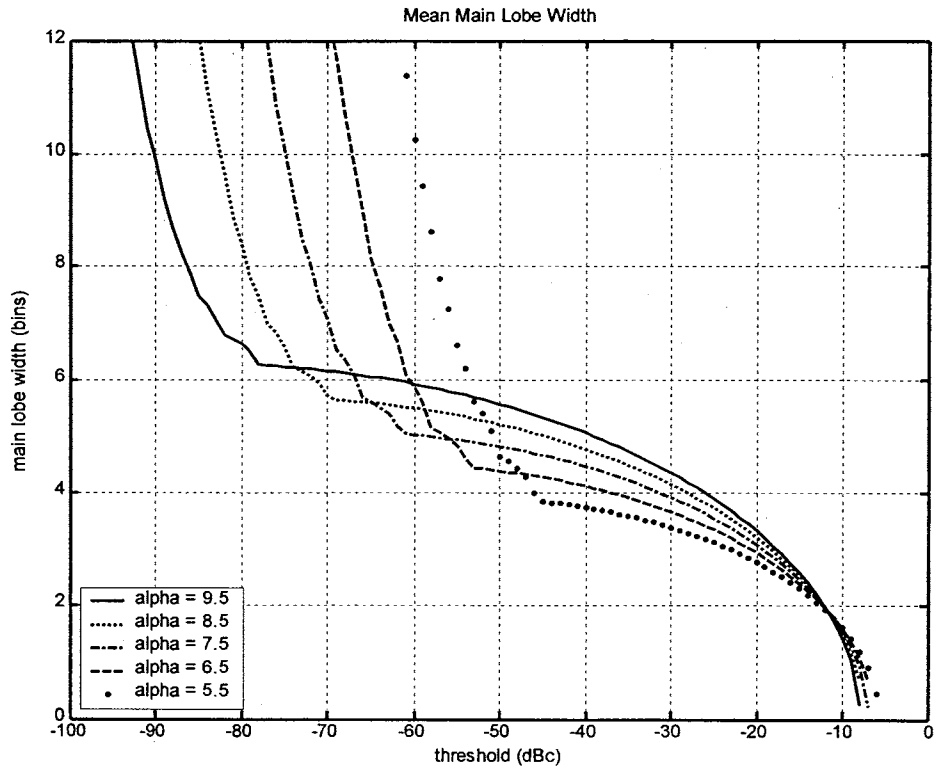

Figure 4. Mean main lobe width vs. threshold for Kaiser windows ($N = 256$)

The same conclusions can be drawn from Figure 4 as can be drawn from Figure 3. Window functions exhibit a breakpoint in excision threshold below which the window function is no longer useful, as its main lobe width increases dramatically. Also, window functions with narrow main lobes tend to have high excision threshold breakpoints. What is noteworthy of the Kaiser window is that its main lobe characteristics can be predictably tuned by adjusting the shape parameter α. This makes the Kaiser window an excellent choice for optimizing a DFT-based excision technique for a particular application.

In summary, excision loss is the loss due to excising part of the desired signal in the process of excising the interference. The main lobe width $M_w(T)$ of the window function $w(n)$ is as a measure of excision loss in terms of the number of DFT bins excised as a function of the excision threshold. This is a useful way of characterizing excision loss independent of the particular characteristics of the desired signal.

Interference Rejection

Interference rejection quantifies the reduction in interference power as a result of excision. Assuming the threshold zeroize excision algorithm referred to previously, any DFT bin is set to zero if it contains interference power exceeding some threshold. While the majority of the interference power will be contained in the excised bins, some fraction of the total interference power remains in the bins that are not excised. The remaining interference power corresponds to the interference rejection achievable by a given DFT-based excisor.

A method to determine the amount of interference power that remains after excision has been developed for the special case of a four-term cosine series window function (Young and Lehnert, 1999). This method derives an expression for the interference power remaining in the side lobes of the DFT for a single interfering tone and a given excision threshold. The side lobes consist of all bins whose powers do not exceed the threshold. The power contained in the side lobes is referred to as side lobe leakage power. The mean side lobe leakage power vs. threshold is computed for a given window function, assuming a uniformly distributed interference frequency.

The side lobe leakage power represents the amount of interference power that remains after excision. Thus, side lobe leakage power is a measure of interference rejection.

A general method for computing mean side lobe leakage power for a particular window function, a given threshold, and a single-tone interferer is presented here. Once again, $W(\omega)$ is the spectrum of the window function $w(n)$:

$$W(\omega) = \sum_{n=0}^{N-1} w(n) e^{-j\omega n}$$

As discussed previously, the function $I_w(\omega, T)$ indicates whether or not the power spectrum $|W(\omega)|^2$ of the window function $w(n)$ exceeds the excision threshold T at a given frequency ω:

$$I_w(\omega, T) = \begin{cases} 1, & |W(\omega)|^2 > T \\ 0, & |W(\omega)|^2 \leq T \end{cases}$$

The side lobes of the spectrum $W(\omega)$ of the window function $w(n)$ consist of all frequencies ω_S that satisfy $I_w(\omega_S, T) = 0$, where $-\pi < \omega_S < \pi$. The side lobe leakage power is computed by integrating the power spectrum $|W(\omega)|^2$ of the window function $w(n)$ over the side lobe frequencies ω_S:

$$S_w(T) = \int_{\omega_S} |W(\omega)|^2 \, d\omega$$

The side lobe leakage power $S_w(T)$ calculated here is the power contained in the side lobes of the power spectrum of the window function $w(n)$, given the threshold T. A single-tone interferer modulated by the window function $w(n)$ has a power spectrum identical to that of the window function shifted to the frequency of

the interferer. As a result, $S_w(T)$ is also the power contained in the side lobes of the power spectrum of a single-tone interferer windowed by $w(n)$. Thus, $S_w(T)$ is the mean side lobe leakage power of the DFT of a single-tone interferer windowed by the function $w(n)$ of length N, given the excision threshold T. As such, the mean side lobe leakage power $S_w(T)$ is as a measure of interference rejection.

The side lobe leakage power $S_w(T)$ can be easily evaluated numerically. The Matlab® computing environment produced by MathWorks, Inc. was used to achieve this. The code used to produce the results given here can be found in the appendix.

Figure 5 shows the side lobe leakage power relative to the threshold vs. excision threshold for several four-term cosine series window functions. The threshold and side lobe leakage power are both normalized to the power present in a single tone interferer with no window applied. The normalized side lobe leakage power (in dBc) is subtracted from the excision threshold (in dBc) to obtain the side lobe leakage power relative to the threshold (in dB). Window functions of length N = 256 were used in these computations, and 2048 equally spaced frequencies per DFT bin were used to approximate the power spectrum of the window function. Once again, it is worth noting that the window length N has no significant effect on these calculations if N is much greater than the main lobe widths of interest. The results in Figure 5 were produced using the method described here and agree with the results given by the special-case method referred to previously (Young and Lehnert, 1999).

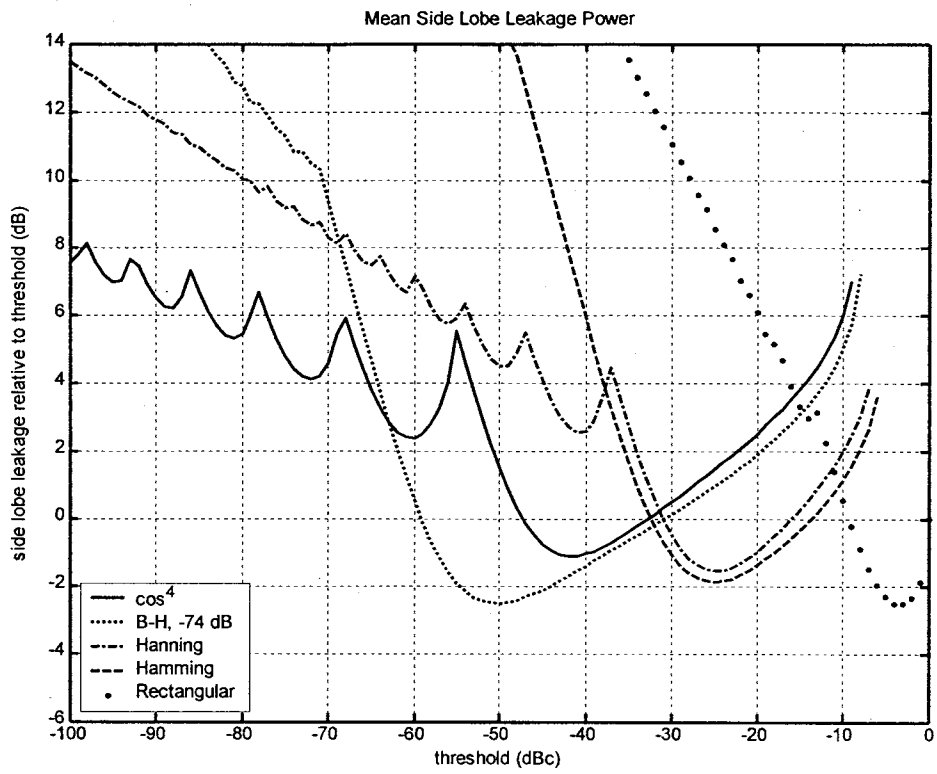

Figure 5. Mean side lobe leakage power vs. threshold for 4-term cosine series windows ($N = 256$)

Upon examining Figure 5, it is evident that each window exhibits a minimum in its side lobe leakage power relative to the excision threshold. This minimum corresponds to the threshold for which the interference rejection is most efficient with respect to the threshold. This is the optimum threshold for use with a particular window function. It is possible to use a threshold lower than the optimum. However, Figure 5 shows that diminishing returns are the result of lowering the excision threshold below the optimum for a given window function.

Comparing Figure 5 to Figure 3, it is apparent that window functions with wider main lobes tend to have lower optimum thresholds and thus better interference rejection performance. For instance, the Hamming window has an optimum threshold of approximately -25 dBc. At this threshold its main lobe width is about 3.0 bins and its side lobe leakage power is about 1.9 dB below the threshold. Thus, the Hamming window provides approximately 26.9 dB of interference rejection at its optimum excision threshold while excising a mean of 3.0 DFT bins. By comparison, the Blackman-Harris window provides about 52.5 dB of interference rejection for a mean main lobe width of about 5.4 bins at an optimum threshold of roughly -50 dBc.

Figure 6 shows the side lobe leakage power relative to the threshold vs. excision threshold for several Kaiser window functions for various values of the shape parameter α. Again, the threshold and side lobe leakage power are both normalized to the power present in a single tone interferer with no window applied. The normalized side lobe leakage power (in dBc) is subtracted from the excision threshold (in dBc) to obtain the side lobe leakage power relative to the threshold (in dB). Window functions of length $N = 256$ were used in these computations, and 2048 equally spaced frequencies per DFT bin were in the approximation of the power spectrum of the window function.

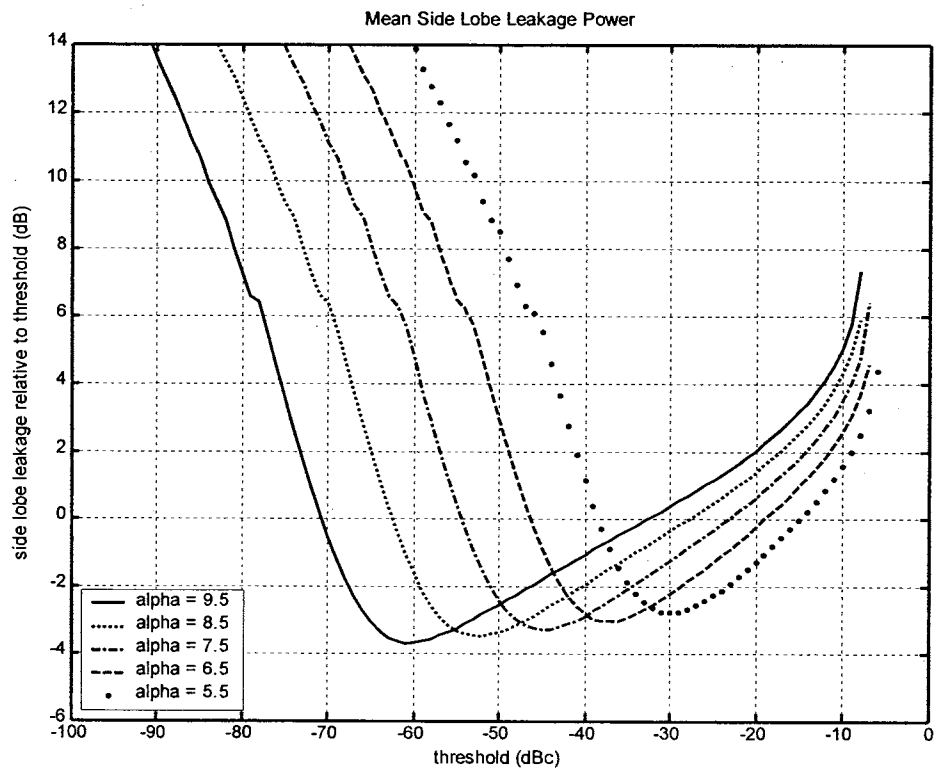

Figure 6. Mean side lobe leakage power vs. threshold for Kaiser windows ($N = 256$)

The same conclusions can be drawn from Figure 6 as can be drawn from Figure 5. Each window function exhibits an optimum excision threshold for which it provides the best side lobe leakage power relative to the threshold. Also, comparing Figure 6 with Figure 4, it is evident that windows with wider main lobes provide better interference rejection performance. It is worth noting that the side lobe leakage characteristics of the Kaiser window can be predictably tuned by adjusting the shape parameter α. As mentioned earlier, this makes the Kaiser window an excellent choice for optimizing a DFT-based excision technique for a particular application.

In summary, interference rejection characterizes the reduction in interference power as a result of excision. The side lobe leakage power $S_w(T)$ of a window function $w(n)$ is a measure of the amount of interferer power, as a function of the excision threshold, that remains after excision is performed. Thus, side lobe leakage power is a useful measure of interference rejection.

APPLICATION TO FH/DSSS SYSTEMS

An overview of DFT-based narrowband interference excision has been given, and the properties of window functions that determine the performance of such an excision technique have been examined. It is now possible to explore how DFT-based excision can be applied in a hybrid frequency-hopping/direct-sequence spread-spectrum (FH/DSSS) system.

A direct-sequence spread-spectrum (DSSS) system uses a pseudorandom sequence to modulate the transmitted signal, typically at a rate that is an integer multiple of the data rate. This has the effect of spreading the spectrum of the transmitted signal by the same integer factor. Thus, a DSSS signal uses a physical bandwidth much greater than the information bandwidth. As a result, a DSSS receiver must be capable of receiving a wideband signal (Proakis and Salehi, 1994). This is what makes a DSSS receiver vulnerable to being desensitized by high-power narrowband signals within its received bandwidth.

A frequency-hopping spread-spectrum (FHSS) system uses a pseudorandom sequence to select the carrier frequency of the transmitted signal. The result is a signal that pseudorandomly hops from one frequency to another, potentially over a very wide band. This requires a FHSS receiver to be very agile in terms of tuning its carrier frequency, depending on the hop rate (Proakis and Salehi, 1994).

When DSSS and FHSS are combined in a hybrid FH/DSSS system, the result is a DSSS signal that is pseudorandomly hopped in frequency. This requires a

receiver that is capable of both receiving a wideband signal and carrier tuning agility. The result is a FH/DSSS receiver that is not only vulnerable to high-power narrowband interference within its received bandwidth. It must also deal with a new interference environment every time it hops to a new carrier frequency. The critical element is the transient nature of the interference as seen by the excision processing. Once this has been addressed, a performance trade-off can be made between loss and interference rejection.

Overlap Transient

Referring to the lower graph in Figure 2, the DFT-based excision technique presented here has a transient response that is $N/2$ samples long for a window function of length N. This is the amount of time it takes the excised signal $x(n)$ to reach its steady state from when the excision processing is begun. The transient response is a result of the 50% overlap-and-add excision architecture. The length of the overlap transient time τ (in seconds) is dependent on the window length N and the sample rate f_s (in samples per second) of the excision processing:

$$\tau = \frac{N}{2f_s}$$

It is reasonable to assume that the interference environment is constant between any two frequency hops, especially for systems with fast hop rates. Ideally, the interference environment seen by the excision processing should be present for the length of the transient response τ before the leading edge of the desired signal

arrives. This would allow the rejection of the interference to settle out before the arrival of the DSSS signal after a given frequency hop. For this to occur, the time between receiver carrier frequency stabilization and the arrival of the desired signal must be greater than the overlap transient time τ.

The overlap transient time τ interacts with a number of FH/DSSS system parameters. One such parameter is tuning time, or how fast a receiver must tune from one carrier frequency to the next during a frequency hop. Another is the amount of off-time allowed during a frequency hop. Off-time is the time before and after a frequency hop during which no signal is transmitted. This typically allows for some tolerance in hop timing between a transmitter and a receiver, as well as propagation delay. Off-time contributes to the overhead of the communication system, reducing the effective amount of information that can be transmitted through a channel. These issues, and possibly others, must be considered in determining the overlap transient time τ allowed in a FH/DSSS system.

It is sufficient for the purposes of this thesis to assume some known allowable overlap transient time τ for the excision. Given this, the length N of the window function must satisfy the following expression:

$$N \leq 2\tau f_s$$

In summary, the transient nature of the interference environment is critical to the application of DFT-based narrowband interference excision in a FH/DSSS system. The maximum length N of the window function is determined by the overlap transient time τ allowed by the system.

Performance Trade-Off

Given a known length N of the window function in a DFT-based excision technique, what remains is the selection of the window function itself. This choice involves a fundamental trade-off in performance between losses incurred and interference rejection achieved. If enhanced interference rejection is desired, the consequences are more windowing loss and more excision loss.

As alluded to previously, the characteristics of the Kaiser window can be predictably tuned by adjusting the shape parameter α. This makes the Kaiser window a flexible choice for DFT-based narrowband excision applications. By simply varying the shape parameter α, a continuous range of performance trade-offs is obtainable. Table 3 contains a summary of Kaiser window properties for several values of the shape parameter α. Included are windowing loss, optimum excision threshold, main lobe width, and interference rejection.

Table 3. Summary of Kaiser window properties

Kaiser window shape parameter	Windowing loss (dB)	Optimum threshold (dBc)	Main lobe width (DFT bins)	Interference rejection (dB)
$\alpha = 5.5$	0.00	-30.0	3.39	32.8
$\alpha = 6.5$	0.01	-37.5	4.03	40.5
$\alpha = 7.5$	0.03	-44.0	4.62	47.3
$\alpha = 8.5$	0.07	-52.0	5.27	55.5
$\alpha = 9.5$	0.13	-61.0	5.95	64.7

The windowing loss shown in Table 3 is the loss for a 50% overlap-and-add DFT-based excision architecture. The windowing loss is also plotted in Figure 7 as a function of the Kaiser window shape parameter α. Note that the windowing loss (in dB) increases exponentially as the shape parameter increases.

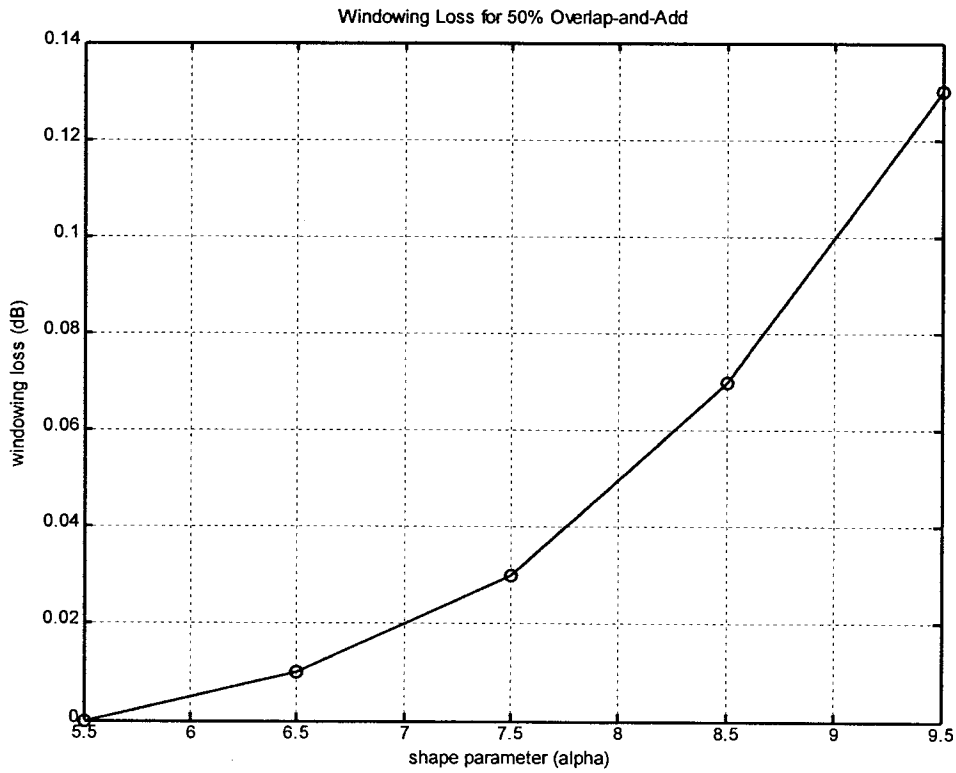

Figure 7. Windowing loss vs. Kaiser window shape parameter α

Recall that the optimum threshold shown in Table 3 is the excision threshold at which the interference rejection is most efficient with respect to the threshold, as can be gathered from Figure 6. The main lobe width found in Table 3 is the mean

main lobe width that occurs at the optimum threshold, as can be gathered from Figure 4. Figure 8 shows the mean main lobe width as a function of the Kaiser window shape parameter α. Note that the main lobe width (in DFT bins) is essentially a linear function of the shape parameter, with the main lobe widening as the shape parameter increases. Recall that main lobe width is the number of DFT bins that must be excised and is therefore a measure of excision loss. Thus, the excision loss increases linearly with the Kaiser window shape parameter.

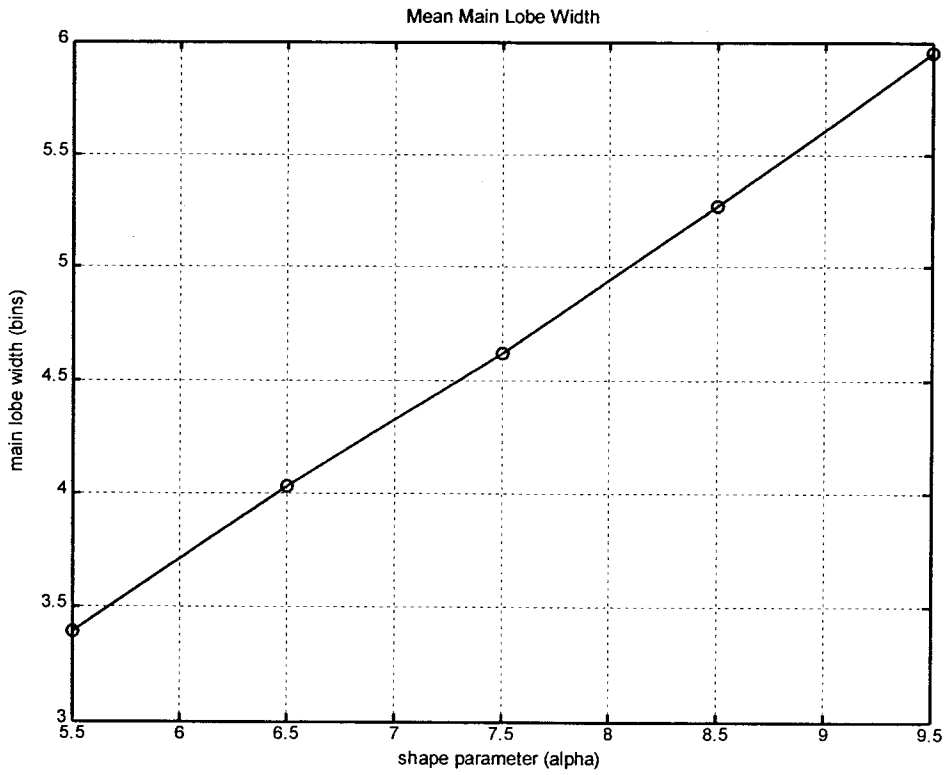

Figure 8. Mean main lobe width vs. Kaiser window shape parameter α

The interference rejection found in Table 3 is the interference rejection achieved for the optimum excision threshold. Recall that interference rejection can be measured in terms of side lobe leakage power. Thus, the interference rejection values (in dB) shown in Table 3 are simply the negation of the corresponding side lobe leakage powers (in dBc). Figure 9 shows interference rejection as a function of the Kaiser window parameter α. Note that interference rejection (in dB) improves linearly as the shape parameter increases.

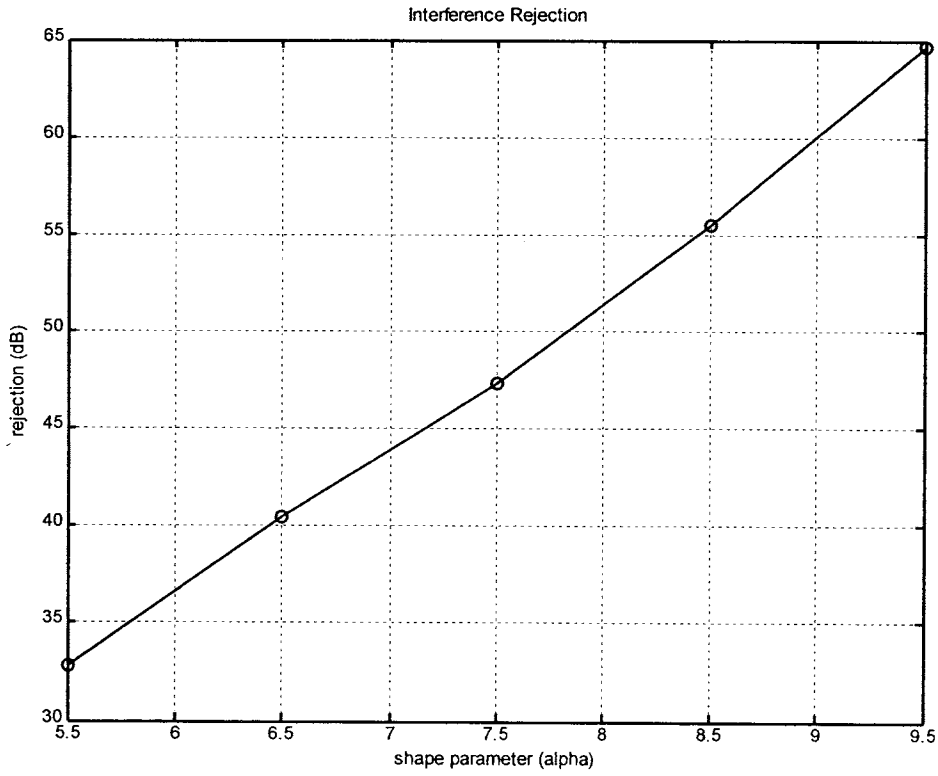

Figure 9. Interference rejection vs. Kaiser window shape parameter α

Figures 7 through 9 depict how windowing loss, main lobe width, and interference rejection depend on the Kaiser window shape parameter α. Figure 10 shows the performance trade-off between windowing loss and interference rejection. Windowing loss (in dB) increases exponentially with increasing interference rejection (in dB). It is important to note that windowing loss is always incurred. It is independent of whether or not interference is being excised, and has the same value regardless of the number of interfering signals being excised.

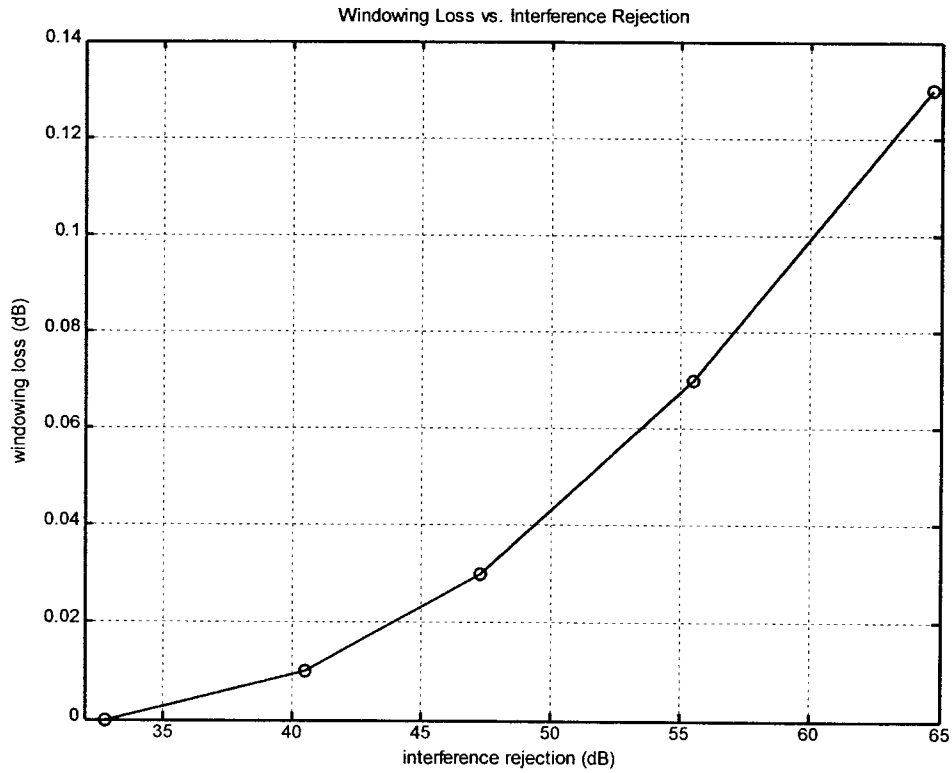

Figure 10. Windowing loss vs. interference rejection

Figure 11 shows the trade-off in performance between excision loss and interference rejection. Excision loss, as measured by main lobe width (in DFT bins), increases linearly with increasing interference rejection (in dB). Approximately 12.5 dB of interference rejection can be achieved for every DFT bin of main lobe width allowed. Unlike windowing loss, excision loss only occurs while interference is being excised. The performance characteristics discussed here are for the case of a single-tone interfering signal. If more than one interfering signal must be excised, then the excision loss will increase commensurately.

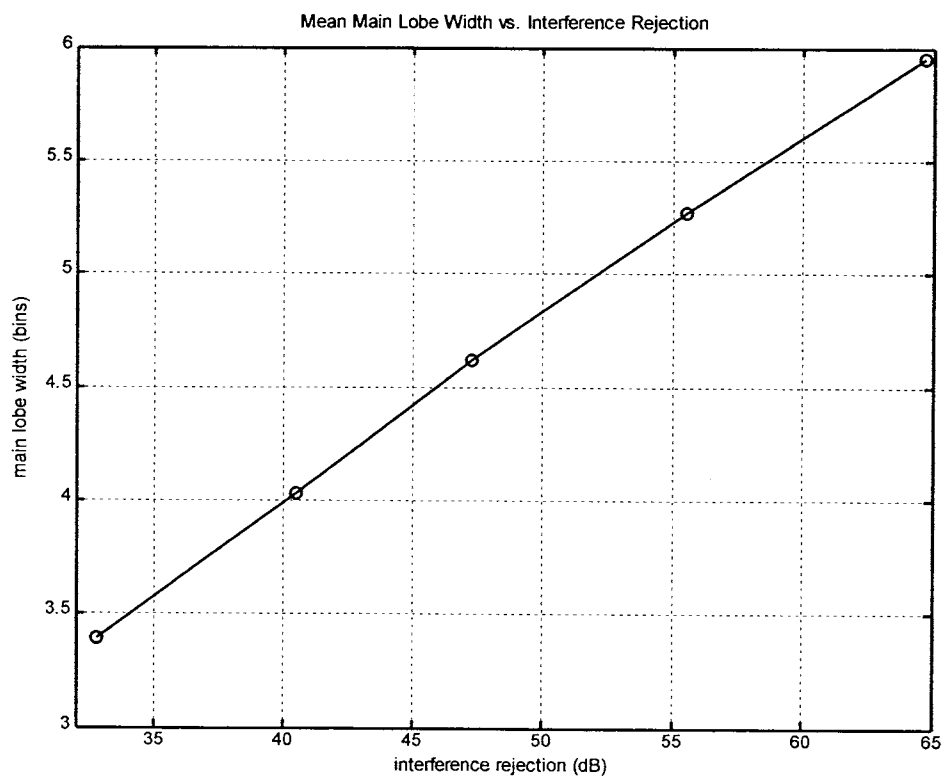

Figure 11. Mean main lobe width vs. interference rejection

For instance, Figure 11 indicates that a mean of approximately 5.6 DFT bins must be excised if a single-tone interfering signal is to be rejected by 60 dB. If two signals must be rejected by the same amount, up to twice the number of bins must be excised, depending on the spacing in frequency of the interfering signals. Thus, up to 11.2 bins must be excised in order to reject two interfering signals by 60 dB.

In summary, a performance trade-off exists between losses incurred and interference rejection achieved in a DFT-based narrowband interference excision scheme. Windowing loss increases exponentially with improved interference rejection, while excision loss increases linearly. Windowing loss is incurred regardless of the interference environment, while excision loss is dependent on the number of interfering signals being excised.

CONCLUSION

This thesis investigated one technique for achieving narrowband interference excision in a hybrid FH/DSSS system. This technique is based on the discrete Fourier transform (DFT). An overview of DFT-based narrowband interference excision was given. This included a brief discussion of excision algorithms and the overlap-and-add architecture used to mitigate the effects of windowing on the time-domain waveform.

Next was a discussion of the properties of window functions that determine the performance of the DFT-based excision technique. These critical properties are windowing loss, excision loss, and interference rejection. Windowing loss is the loss in signal-to-noise ratio (SNR) resulting from the time-domain shape of the window function. Excision loss is the loss due to excising part of the desired signal in the process of excising the interference. Interference rejection is the reduction in interference power as a result of excision.

Finally, the application of DFT-based excision in a hybrid FH/DSSS system was explored. The critical element is the transient nature of the interference as seen by the excision processing. This determines the maximum length of the window function. Once this is known, a performance trade-off can be made between loss and interference rejection.

Future work may include investigation of practical issues related to implementing narrowband interference excision in a communication system. Such

issues include the effects of synthesizer phase noise, receiver spurious responses, and signal quantization. Future work may also include the exploration of alternate excision methods, such as parametric interference modeling and parametric excision.

APPENDIX

Matlab Script: WindowAnalysis.m

```
%   Analysis of DFT Windows
%
%   Carlos J Chávez
%   11/2002
%   last revision:  12/9/2002


N = 256;            %   length of window
LtoN = 2048;        %   number of frequency samples per frequency bin


%   frequency vector

L = LtoN*N;         %   number of frequency samples
fs = N;             %   sample rate (normalized to number of frequency bins)

df = fs/L;
f = -fs/2 : df : (fs/2 - df);

%   time vector (samples)

n = 0 : (N - 1);


%   threshold vector (dBc, relative to total power in a complex exponential)

ThreshMin = -100;
ThreshStep = 1;
Threshold = ThreshMin : ThreshStep : 0;
N_Thresh = length(Threshold);


%   window function

% a = [ 0.35875 0.48829 0.14128 0.01168 ];        %   Blackman-Harris, -92 dB
% a = [ 0.40217 0.49703 0.09392 0.000183 ];       %   Blackman-Harris, -74 dB
% a = [ 0.42323 0.49755 0.07922 0 ];              %   Blackman-Harris, -67 dB
% a = [ 0.44959 0.49364 0.05677 0 ];              %   Blackman-Harris, -61 dB
% a = [ 0.42 0.5 0.08 0 ];                        %   Blackman
% a = [ 0.31250 0.46875 0.18750 0.03125 ];        %   cos6
% a = [ 0.375 0.5 0.125 0 ];                      %   cos4
% a = [ 0.5 0.5 0 0 ];                            %   Hanning
% a = [ 0.54 0.46 0 0 ];                          %   Hamming
% a = [ 1 0 0 0 ];                                %   rectangular
% w = win4cs(N, a);

a = 5.5;
w = kaiserwin(N, a);


%   window parameters

Gnp = sum(w.^2)/N;      %   noise power gain
Gpp = (sum(w)/N)^2;     %   peak power gain

Beq = Gnp/Gpp;          %   equivalent noise bandwidth (bins)
```

```
%   effective window for 50% overlap

w_over = w + fftshift(w);


%   window parameters for 50% overlap

Gnp_over = sum(w_over.^2)/N;        %   noise power gain
Gpp_over = (sum(w_over)/N)^2;       %   peak power gain

Beq_over = Gnp_over/Gpp_over;       %   equivalent noise bandwidth (bins)


%   window frequency response (normalized)

G = abs(freqz(w, 1, f, fs)/N).^2;
GdB = 10*log10(abs(G));


%   mean main lobe width

MainLobe = [];
for k = 1 : N_Thresh
    MainLobe(k) = length(find(GdB > Threshold(k)))/LtoN;
end


%   mean side lobe leakage power (normalized to total power)

SideLobePower = [];
for k = 1 : N_Thresh
    i = find(GdB <= Threshold(k));
    SideLobePower(k) = sum(G(i));
end
SideLobePower = SideLobePower/sum(G);


%   output

Beq_dB = 10*log10(Beq)
Beq_over_dB = 10*log10(Beq_over)

figure(1);
plot(n, w, n, fftshift(w), n, w_over);
grid on; zoom on;
axis([ 0 N 0 max(w_over) ]);
title('Window Function With 50% Overlap');
xlabel('time (samples)');
ylabel('amplitude');

figure(2);
plot(f, GdB);
grid on; zoom on;
axis([ -fs/2 fs/2 -110 0 ]);
title('Window Function');
xlabel('frequency (bins)');
ylabel('magnitude response (dB)');

figure(3);
plot(Threshold, MainLobe);
grid on; zoom on;
axis([ ThreshMin 0 0 12 ]);
title('Mean Main Lobe Width');
xlabel('threshold (dBc)');
ylabel('main lobe width (bins)');
```

```
figure(4);
plot(Threshold, 10*log10(SideLobePower), Threshold, Threshold, 'k:');
grid on; zoom on;
axis([ ThreshMin 0 -100 0 ]);
title('Mean Side Lobe Leakage Power');
xlabel('threshold (dBc)');
ylabel('side lobe leakage (dBc)');

figure(5);
plot(Threshold, 10*log10(SideLobePower) - Threshold);
grid on; zoom on;
axis([ ThreshMin 0 -6 14 ]);
title('Mean Side Lobe Leakage Power');
xlabel('threshold (dBc)');
ylabel('side lobe leakage relative to threshold (dB)');
```

Matlab Function: win4cs.m

```
function w = win4cs(n, a)
%   4-Term Cosine Series Window
%
%   Carlos Chávez
%   11/2002
%   last revision:  11/27/2002
%
%   W = WIN4CS(N, A) returns the N-point 4-term cosine series window in a row
%   vector.  A must be a vector of length 4 containing the four-term cosine series
%   coefficients for the desired window.
%
%   A = [ 0.35875 0.48829 0.14128 0.01168 ];        %   Blackman-Harris, -92 dB
%   A = [ 0.40217 0.49703 0.09392 0.000183 ];       %   Blackman-Harris, -74 dB
%   A = [ 0.42323 0.49755 0.07922 0 ];              %   Blackman-Harris, -67 dB
%   A = [ 0.44959 0.49364 0.05677 0 ];              %   Blackman-Harris, -61 dB
%   A = [ 0.42 0.5 0.08 0 ];                        %   Blackman
%   A = [ 0.31250 0.46875 0.18750 0.03125 ];        %   cos6
%   A = [ 0.375 0.5 0.125 0 ];                      %   cos4
%   A = [ 0.5 0.5 0 0 ];                            %   Hanning
%   A = [ 0.54 0.46 0 0 ];                          %   Hamming
%   A = [ 1 0 0 0 ];                                %   rectangular


x = (0 : n - 1) + 0.5;

w = a(1) - a(2)*cos(2*pi*x/n) + a(3)*cos(4*pi*x/n) - a(4)*cos(6*pi*x/n);
```

Matlab Function: kaiserwin.m

```
function w = kaiserwin(n, alpha)
%   Kaiser Window
%
%   Carlos Chávez
%   11/2002
%   last revision:  12/1/2002
%
%   W = KAISERWIN(N, ALPHA) returns the ALPHA-valued N-point Kaiser window in a
%   row vector.


x = (0 : n - 1) + 0.5;

w = besseli(0, alpha*sqrt(1 - (x - (n/2)).^2/(n/2)^2))...
    /besseli(0, alpha);
```

REFERENCES

F. J. Harris, "On the use of windows for harmonic analysis with the discrete Fourier transform," *Proc. IEEE*, vol. 66, pp. 51-83, January 1978.

S. J. Orfanidis, *Introduction to Signal Processing*. Upper Saddle River, NJ: Prentice-Hall, 1996.

J. G. Proakis and D. G. Manolakis, *Digital Signal Processing: Principles, Algorithms, and Applications*. Upper Saddle River, NJ: Prentice-Hall, 1996.

J. G. Proakis and Masoud Salehi, *Communication Systems Engineering*. Upper Saddle River, NJ: Prentice-Hall, 1994.

J. A. Young and J. S. Lehnert, "Analysis of DFT-based frequency excision algorithms for direct-sequence spread-spectrum communications," *IEEE Trans. Commun.*, vol. 46, no. 8, pp. 1076-1087, August 1998.

J. A. Young and J. S. Lehnert, "Performance metrics for windows used in real-time DFT-based multiple-tone frequency excision," *IEEE Trans. Signal Processing*, vol. 47, no. 3, pp. 800-812, March 1999.